PAPER

Check for updates

An extracellular matrix-mimicking magnetic microrobot for targeted elimination of circulating cancer cells†

Jing Huang,‡[a,b] Yuan Liu,‡[b] Jiandong Wu, [ID][b] Fuping Dong, [ID] *[a] Chu Liu,[b] Jiawei Luo,[b] Xiangchao Liu,[b] Ning Wang,[b] Lei Wang[b] and Haifeng Xu [ID] *[b]

Cancer cells disseminate through the bloodstream, leading to metastasis in distant sites within the body. One promising strategy to prevent metastasis is to eliminate circulating tumor cells. However, this remains challenging due to the lack of an active and targeted biomedical tool for efficient cancer cell elimination. Here, we developed a magnetic microrobot by using natural materials derived from the extracellular matrix (ECM) to mimic the ligand–receptor interaction between cancer cells and the ECM, offering targeted elimination of cancer cells. The ECM-mimicking microrobot is designed with a biodegradable hydrogel matrix, incorporating a cancer cell ligand and magnetic microparticles for cancer cell capture and active locomotion. This microrobot was fabricated based on an interface-shearing method, enabling controllable magnetic response and size scalability (30 µm–500 µm). The presented ECM-mimicking microrobot can actively approach and capture single cancer cells and cell clusters under the control of specific magnetic fields. The experiment was conducted in a blood vessel-mimicking simulator. The microrobot demonstrates an outstanding elimination efficacy of 92.3% on MDA-MB-231 cancer cells and a stable transport capability of the captured cells over long distances to a designed recycling site, inhibiting cell metastasis. This magnetic ECM-mimicking microrobot based on a bioinspired binding mechanism represents a promising candidate for the efficient elimination of cancer cells and other biological waste in the blood.

1. Introduction

Cancer metastasis accounts for over 90% of cancer-related deaths.[1–4] As key precursors of cancer metastasis, circulating tumor cells (CTCs) that are shed from primary tumor sites can disseminate through the bloodstream and damage distant organs.[5–7] Eliminating CTCs is regarded as a promising strategy to prevent cancer metastasis yet it remains extremely challenging due to the lack of an effective biomedical tool with combined functions of active targeting and efficient elimination towards cancer cells. Existing therapeutic approaches, such as chemotherapy,[8] surgery[9] and radiotherapy[10] were developed to mainly treat the primary tumor cells and often induce severe side effects like nausea, fatigue, anemia, and infection.[11] A gentler and safer therapeutic approach to eliminate CTCs is urgently needed.

In this pursuit, devices that mimic the natural extracellular matrix (ECM) offer promising avenues to collect CTCs for cancer metastasis treatment.[12–14] The ECM is a highly complex fibrous network composed of various biomacromolecules, such as proteins, glycosaminoglycans and glycoconjugates,[15–17] providing the dynamic ligand–receptor interaction with various types of cells.[18,19] Specifically, hyaluronic acid (HA), as one of the main functional components of the ECM, enables a selective ligand–receptor interaction with the CD44 receptor overexpressed in cancer cells.[20,21] Hence, mimicking the dynamic interaction between ECM ligands and cancer cells holds the potential to selectively recognize and collect CTCs. Employing the intrinsic function of those biogenic materials could efficiently trigger relevant cell behaviours like cell adhesion.[22–24] Previously, ECM-mimicking microbeads, such as phenylboronic acid (PBA)-functionalized magnetic microbeads[25] and cancer peptide-modified magnetic microbeads,[26] were developed with the function of cell–material interactions, showing high cancer cell selectivity and potential for early cancer diagnosis and prognosis.[27] However, present passive microbeads lack the mobility required for

[a] Department of Polymer Materials and Engineering, College of Materials and Metallurgy, Guizhou University, Guiyang, 550025, China. E-mail: fpdong@gzu.edu.cn
[b] Shenzhen Institute of Advanced Technology, Chinese Academy of Science, Shenzhen, 518055, China. E-mail: hf.xu@siat.ac.cn
† Electronic supplementary information (ESI) available. See DOI: https://doi.org/10.1039/d3nr03799a
‡ These authors contributed equally to this work.

active cancer cell capture and elimination from the bloodstream *in vivo*. Recently, magnetic microrobots have emerged as potent active treatment strategies *in vivo*,[28–30] showcasing their remarkable ability to execute diverse biomedical tasks,[31] such as cargo transport,[32–34] minimally invasive surgery[35,36] and sensing.[37] Particularly, pollen-based microrobots[38] and Janus-particle-based microrobots[39] were developed to attach cancer cells by electrostatic force. However, a microrobot with function comparable to the ECM is still unavailable.

To address these above limitations, we present a magnetic microrobot based on ECM-derived materials for the targeted elimination of cancer cells *in vivo* within venous vessels.[40] As shown in Fig. 1A, the spherical ECM-mimicking microrobot consists of a gelatin matrix embedded with HA blocks and NdFeB magnetic particles. As the main component of the ECM,[15] HA provides the ligand–receptor interaction with the cancer cells for the microrobot while the gelatin matrix ensures biocompatibility and biodegradability.[41] The embedded magnetic particles offer strong magnetic torque for actuation under external magnetic fields. The present ECM-mimicking microrobot can actively approach, capture and transport target cancer cells to a designed recycling site, inhibiting cancer metastasis (Fig. 1B). This active elimination strategy represents a gentle and safe way with minimal side effects to treat cancer metastasis.

2. Results and discussion

2.1 Fabrication of the magnetic ECM-mimicking microrobot

Fig. 2A depicts the fabrication process of the magnetic ECM-mimicking microrobots based on an "interface-shearing method", which enables microrobots with scalable dimensions and controllable magnetic content. The microrobot-generating system consists of a syringe with a microneedle of 150 μm inner diameter, a linkage rod, and a pressure rod. The syringe stores the HA/gelatin/NdFeB prepolymer, of which HA is preliminarily cross-linked by 1-ethyl-3-(3-dimethyl-aminopropyl) carbodiimide (EDC) to improve its stability and mechanical properties.[42,43] The pressure rod provides controllable flow speeds for the prepolymer by pressing the syringe. The linkage rod provides the frequency to move up and down, which results in the interaction between the prepolymer droplet and the air/oil interface. The frequency (f) of the microneedle plunging inside the oil phase can be modulated in the range of 1–6 Hz. The HA/gelatin/NdFeB microspheres are successfully generated by shearing the prepolymer droplets at the air–oil interface. Fig. 2B further depicts the mechanical analysis of the generation process of the HA/gelatin/NdFeB droplets. The shear force (F_s) and interfacial force (F_i) affect the droplet-generation process.[44] F_i is directly proportional to the width of the droplet neck l, which resists droplet expansion and detachment. F_s is proportional to the product of the microneedle diameter (d) and the plunge speed (Q_c) of the linkage rod, leading to the squeezing of the prepolymer at the outlet of the microneedle. After washing (Fig. S1†), the produced HA/gelatin/NdFeB microspheres can be stably stored in phosphate-buffered saline (PBS). Fig. 2C shows further validation of the magnetic properties of the proposed ECM-mimicking microrobot, as microrobots dispersed in the buffer are shown to aggregate to one side under the influence of a permanent magnet. Thus, the magnetic ECM-mimicking microrobots, characterized by their spherical shape and the
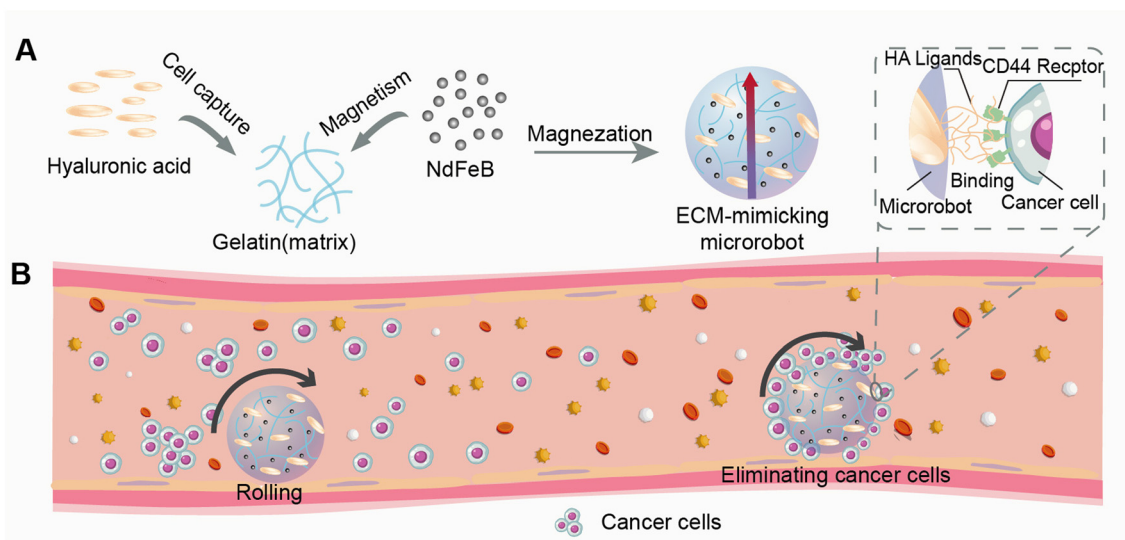

Fig. 1 Concept of targeted cancer cell elimination in the blood vessel using the magnetic ECM-mimicking microrobot. (A) Schematic of the internal structure of the microrobot, composed of a gelatin matrix, hyaluronic acid, and magnetic nanoparticles. Upon magnetization, the microrobot aligns its magnetization dipole toward the direction of the magnetic field, indicated by the arrow. (B) Conceptual schematic showing the working mechanism of the magnetic ECM-mimicking microrobot rolling within the blood vessel and eliminating cancer cells. The selective recognition and adhesion of cancer cells are through the interaction between the HA ligands and CD44 receptor, endowing the microrobot with autonomous targeting capability.
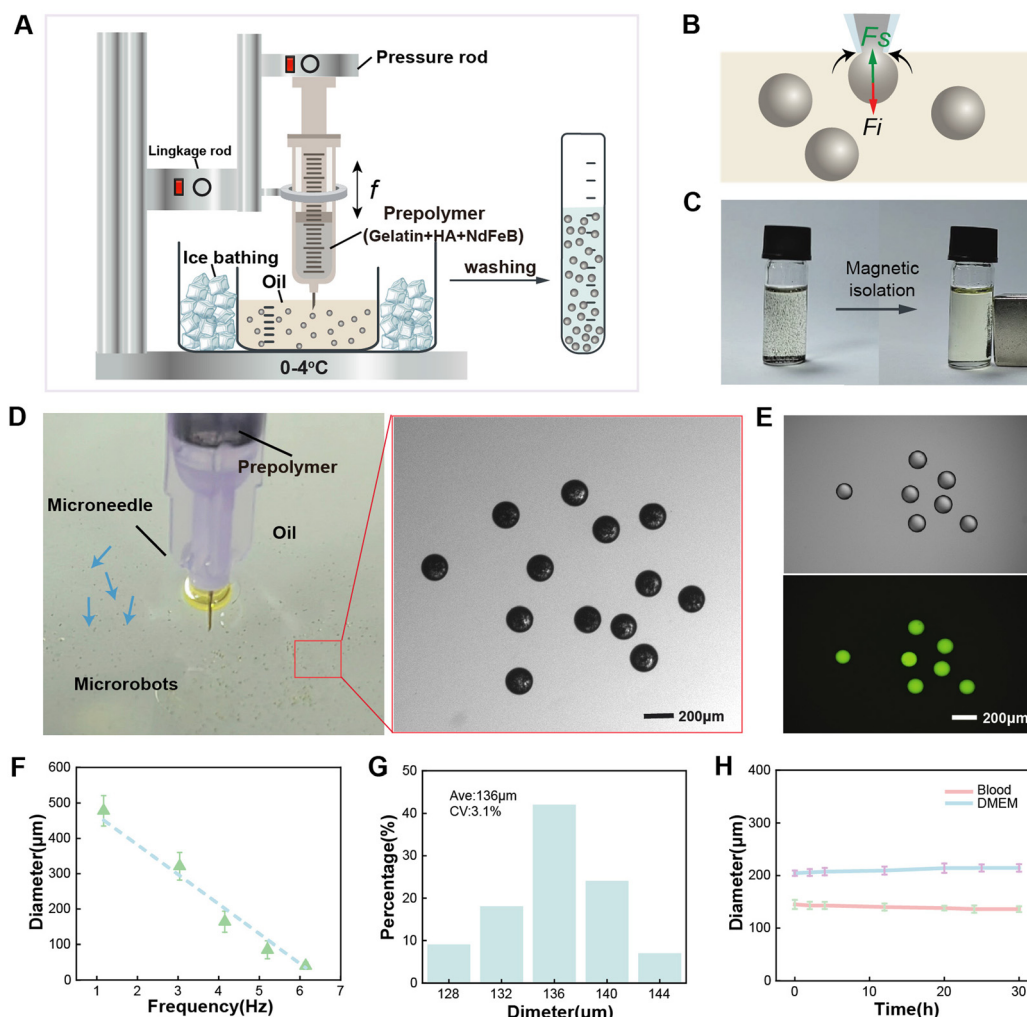
Fig. 2 Characterization of the magnetic ECM-mimicking microrobot. (A) The fabrication process of the microrobot by the "interface-shearing" method utilizing a droplet-generating device. (B) Droplet-generation mechanism. (C) Magnetic isolation of microrobots from the oil phase. (D) Mass production of the magnetic ECM-mimicking microrobot. Blue arrows indicate four suspended microrobots out of a massive number of them observed as black microparticles in the solution, showcasing their uniform dimensions. (E) Fluorescence images of the encapsulated fluorescence-labelled hyaluronic acid (HA) in the microrobot. Ex: 496 nm and Em: 522 nm. (F) Size distribution of the magnetic ECM-mimicking microrobot fabricated at frequencies ranging from 1 Hz to 6 Hz; $n = 12$ samples, mean $\pm$ sd. (G) Coefficient of variation (CV) analysis of the magnetic ECM-mimicking microrobot at a plunging frequency of 4.91 Hz. (H) Stability assessment of the magnetic ECM-mimicking microrobot in blood and cell culture media; $n = 3$ samples, mean $\pm$ sd.

uniform distribution of magnetic particles, are successfully produced using the interface-shearing method. Fig. 2D illustrates the fabricated magnetic ECM-mimicking microrobots with smooth spherical morphology. The utilization of ice bathing for rapid cooling of the gelatin matrix during the generation process prevents the microrobot droplets from adhering to each other. Fig. 2E shows the successful incorporation of HA inside the gelatin matrix after fabrication by using fluorescence-labelled HA as an indicator. As shown in Fig. 2F and Fig. S2,† the diameter of the microrobot ranges from 30 μm to 500 μm, corresponding to the needle plunging frequency dropping from 6 Hz to 1 Hz. We evaluate the microrobots' diameters by altering the plunge frequency, revealing a clear linear dependence ($r = 0.96$), signifying that adjusting the

needle plunging frequency facilitates precise control over the magnetic spherical ECM-mimicking microrobot's dimensions. At a plunge frequency of 4.91 Hz, the microrobot possesses an average diameter of 136 μm with a coefficient of variation of approximately 3.1% (Fig. 2G). The size dispersity can be attributed to the fluctuations in the flow speed and plunge frequency. Furthermore, relying on its constitution of body-derived materials, the magnetic ECM-mimicking microrobot with a low zeta potential (−32 mV) demonstrates high biosafety (Fig. S3†), inducing minimal hemolysis (Fig. S4†). The stability in the blood and biological solutions is also crucial for designing biomedical microrobots. Fig. 2H and Fig. S5† present the swelling resistance of the magnetic ECM-mimicking microrobots in blood and cell culture media over 30 hours. The cross-

linked microbots can stably retain their spherical shape, and the diameter of the microrobot is almost stable.

2.2 Magnetic actuation

To characterize the essential magnetic properties for actuation, a vibrating sample magnetometer (VSM) with a hysteresis cycle between +2 T and −2 T is used to obtain the magnetization of the fabricated magnetic ECM-mimicking microrobot. The hysteresis loop in shown Fig. 3A indicates that the fabricated microrobots exhibit a hard magnetic behavior. For the magnetic actuation, the microrobots are pre-magnetized under 1 T. The actuation field strength is 1 mT. The magnetic ECM-mimicking microrobot derives magnetic torque from the contained NdFeB particles, expressed as the following:

$$T = V \cdot M \times B \tag{1}$$

where V and M are the volume and the magnetization of the material, respectively, and B is the external applied magnetic field. The magnetic ECM-mimicking microrobot's speed relies on the applied magnetic field and the volume of NdFeB mag-

netic particles. The motion direction of the microorbot can be modulated by changing the orientation of the rotating magnetic field. Under the actuation of a rotating magnetic field, the magnetic ECM-mimicking microrobots can rotate to move forward. The friction force induced by the substrate provides sufficient propelling force to actuate the microrobots under a magnetic field of down to 1 mT and a frequency of 0.1 Hz. The speed of the microrobot before the step-out is correlated to the rotation frequency of the external field ω and the diameter r of the microrobot by eqn (2):[45]

$$v = 2\pi r\omega \tag{2}$$

where r is the radius of the microrobot and ω is the rotation frequency of the applied magnetic field B. Fig. 3B reveals that the speed of the magnetic ECM-mimicking microrobot increases linearly with the applied frequency before the step-out frequency. In addition, under the same driving frequency, the magnetic ECM-mimicking microrobot with a larger diameter leads to a higher motion speed. Fig. 3C and Video S1† show the precise directional control of the magnetic ECM-

Fig. 3 Magnetic control of the magnetic ECM-mimicking microrobot under a rolling motion. (A) Magnetic properties measured using a vibrating sample magnetometer (VSM), confirming the microrobot's magnetization behaviour. The hysteresis loop indicates a hard magnetic behaviour, with an intrinsic magnetization maximum of 22.84 emu g⁻¹ achieved at a maximum field of 1.96 T. The remanent magnetization is 15.4 emu g⁻¹, and the coercive field is 400 mT. (B) The microrobot velocity increasing with the frequency of the magnetic field before stepping out. Plots show microrobots with different diameters (140 μm, 200 μm, and 280 μm) under an applied 1 mT magnetic field. The data indicate a linear correlation between the motion speed and the frequency within the considered range. Error bars represent standard deviation, n = 3 samples, mean ± sd. (C) The trajectory of the controlled microrobot following a preset rectangular path, demonstrating the precise directional control capability. (D) Magnetic control of the microrobot in the cell culture medium. The purple line indicates the microrobot's trajectory.

mimicking microrobot in water at 0.2 Hz and 1 mT. As a result, the magnetic ECM-mimicking microrobot could freely follow the direction of the magnetic field and reach controllable locations along the predefined rectangular track. Furthermore, we assessed the microrobot performance in a cell culture medium (DMEM) with suspended cancer cells. Fig. 3D shows that the ECM-mimicking microrobot demonstrates a stable magnetic actuation behaviour in the cell culture medium with suspended cancer cells and cell clusters (as also shown in Video S2†). The velocity reaches 142.9 μm s^{-1}. This demonstrates that the cancer cells in the culture medium show little influence on the translational motion of the microrobot.

2.3 Targeted capture of cancer cells

We demonstrate the cell capture capabilities of the magnetic ECM-mimicking microrobot using MDA-MB-231 (triple negative human breast cancer cell line) as the target cancer cells. MDA-MB-231 cells are incubated with DMEM buffer in the incubator at 37 °C under a humidified atmosphere supplied with 5% CO$_2$. After being washed three times with detergent

and deionized water, the microrobots are added to the DMEM containing suspended cancer cells (5×10^4 cells per mL). The magnetic ECM-mimicking microrobot exhibits intriguing cell capture behavior during the rolling motion, enabling it to naturally capture both single cancer cells and cell clusters. In Fig. 4A and Video S3,† we observe the targeted capture of a single cancer cell. The microrobot dynamically adjusts its translational velocity and direction to approach the cancer cell before making direct contact. At $T = 8$ s, the microrobot successfully captures the cell and rolls forward with it. Fig. 4B and Video S3† demonstrate the magnetic ECM-mimicking microrobot's movement toward a cancer cell cluster at a speed of 107 μm s^{-1} under the same magnetic control parameters. At $T = 5$ s, the microrobot effectively captures the cancer cell cluster, carrying it to move forward. Remarkably, during both single-cell and cluster capture processes, we observe no significant cell detachment, indicating a strong binding force between the microrobot and cancer cells.

To further evaluate this binding force, we subjected the magnetic ECM-mimicking microrobot adhering to cancer cells to spin under a 1 mT rotating magnetic field at a higher fre-

Fig. 4 Demonstration of cancer cell capture by the magnetic ECM-mimicking microrobot. (A) Time-lapse images illustrating the capturing process of a single cancer cell. (B) Time-lapse images illustrating the capturing of a cancer cell cluster. The microrobot effectively captures the cell cluster by rolling over it and maintaining a strong binding force with the cancer cells. (C) Statistical analysis of cancer cells captured by magnetic ECM-mimicking microrobots of different sizes. The number of captured cancer cells is quantified for microrobots with diameters of 150 μm, 214 μm, and 320 μm, demonstrating a positive relationship between microrobot size and capture capacity. (D) Targeted elimination of cancer cells in a predefined area. The purple arrows indicate the trajectory and movement directions of the microrobot during the elimination process. (E) The specificity of the magnetic ECM-mimicking microrobot on collecting cancer cells in the blood. (F) Live/dead staining of the cells cultured with the magnetic ECM-mimicking microrobot for 48 h.

quency of 6 Hz (Video S4†). The captured cancer cells are stably adhered to the microrobot without detachment thanks to the robust binding. To explore the capture capability of the magnetic ECM-mimicking microrobots with different dimensions, we selected microrobots with varying diameters and recorded the number of captured cells when reaching the maximum capacity. Fig. 4C shows that the magnetic ECM-mimicking microrobots with diameters of 150 μm, 214 μm, and 320 μm capture 28, 46, and 61 cancer cells, respectively, indicating the increasing cell-capturing capacity with the increasing microrobot diameter. Furthermore, we demonstrated the cell elimination capability of the microrobot within a constrained region. As shown in Fig. 4D and Video S3,† the microrobot successfully captures 41 cancer cells out of 46 cells suspended in a 764 μm × 489 μm area during 85 s of continuous working. To further certify the targeting proficiency of our microrobots with tumor cells, we conducted a cell elimination experiment in the blood. The magnetic ECM-mimicking microrobot was injected into the whole blood to capture cancer cells at 0.3 Hz and 3 mT. As shown in Fig. 4E and Video S5,† the microrobot effectively captures 8 cancer cells within a remarkably short time of 5 minutes. Importantly, throughout the entire process of capturing cancer cells, the magnetic ECM-mimicking microrobot does not adhere to other blood components, such as red blood cells, white blood cells, and other immune cells, confirming its precise targeting effect on tumor cells. HA plays a specific role in cancer cell selectivity of the microrobot. As a comparison, the pure gelatin microbead is not capable of adhering to cancer cells (Fig. S6 and Fig. S7†). These findings highlight the effective capturing capability of the magnetic ECM-mimicking microrobot toward cancer cells, driven by its selective binding and active robotic locomotion. In the future application of such microrobots, biocompatibility will be a vital factor for them to operate *in vivo*. We present the biocompatibility of our microrobots through the cell viability test by incubating cancer cells with them. As shown in Fig. 4F and Fig. S8,† after 48 h of culture, cells are spread over the well adopting their typically spindle-shaped morphology. The cell viability remained stable. These results demonstrate that the magnetic ECM-mimicking microrobot inflicts very low cell damage.

2.4 Effective elimination of cancer cells by the magnetic ECM-mimicking microrobot

To demonstrate the capability of the magnetic ECM-mimicking microrobot to effectively eliminate cancer cells, a dumbbell-shaped microfluidic chip mimicking a blood vessel is used as the working platform for the microrobot to perform the cell elimination and transport tasks (Fig. 5A). The mimicking simulator, with a microchannel height of 2 mm, is designed with two chambers (4 mm in diameter) connected *via* a narrow channel (1 mm in width and 2 mm in length). In this setup, the left chamber, middle channel and right chamber represent the elimination area (the dotted area), the transport channel, and the recycling site, respectively. As shown in Fig. 5A, MDA-MB-231 cancer cells are cultured in the left chamber at a

concentration of 5×10^4 cells per mL, while the transport channel and the right chamber remain free of cancer cells. The magnetic ECM-mimicking microrobot is carefully introduced into the left chamber by micro-pipetting. Time-lapse image sequences of the magnetic ECM-mimicking microrobot's locomotion to eliminate and transport the MDA-MB-231 cells are shown in Fig. 5B and Video S6.† The red points in Fig. 5B mark the position of the magnetic ECM-mimicking microrobot in the microchip. Before eliminating ($T = 0$ min), the microrobot locates itself at the initial position without any captured cancer cells. Under a rotating 2 mT magnetic field at 0.1 Hz, the magnetic ECM-mimicking microrobot exhibits smooth movement along the defined path to collect the suspended cells. As expected, after a certain time for capturing ($T = 20.33$ min), the magnetic ECM-mimicking microrobot accomplishes an impressive cell collection efficiency of 92.3% in the elimination area highlighted inside the dotted oval (Fig. 5B, i). During the transport process (Fig. 5B, ii), the magnetic ECM-mimicking microrobot is guided to move into the transport channel, and the magnetic ECM-mimicking microrobot with captured cells is guided to rapidly move towards the desired location at a speed of 118 μm s^{-1}. After 29 s (Fig. 5B, iii) of rolling, the magnetic ECM-mimicking microrobot transports the cancer cells to the recycling chamber. In a real treatment situation in the future, the microrobots with captured cells can be taken out of the body from the recycling sites by means of conventional microsurgery instruments, such as an endoscope or an interventional microcatheter, as reported in previous successful cross-scale robotics studies.[46–48] During the process of eliminating cancer cells in the microfluidic channel within 22.33 min, neither cancer cell detachment nor microrobot collapse occurs, which further indicates the large binding force between the microrobot and cancer cell and the stability of the microrobot. These above-mentioned results effectively verify that the designed microrobot can actively capture and precisely transport cancer cells under an external magnetic field, facilitating the final cancer cell elimination.

2.5 Magnetically driven locomotion of the magnetic ECM-mimicking microrobot *in vivo*

To investigate the potential application and feasibility of the magnetic ECM-mimicking microrobot *in vivo*, we injected our ECM-mimicking microrobot into the jugular vein of a rat. A digital radiography (DR) X-ray system was equipped for monitoring the microrobot in the blood vessels *in situ*. Briefly, we injected a microrobot into the pre-ligated vein with a length of 1 cm (Fig. S9†). To minimize the interference from imaging noise during the experiment, we chose the microrobot with a relatively large diameter of 500 μm as our model sample. As viewed from the X-ray imaging, the position of the marked microrobot can be accurately tracked within the neck vein of the rat model. Movement of the magnetic ECM-mimicking microrobot was then initiated in the vein under the actuation of an external magnetic field. The position change of the magnetically driven microrobot could be recorded every 10 seconds. As shown in Fig. 6, the microrobot moves at a speed
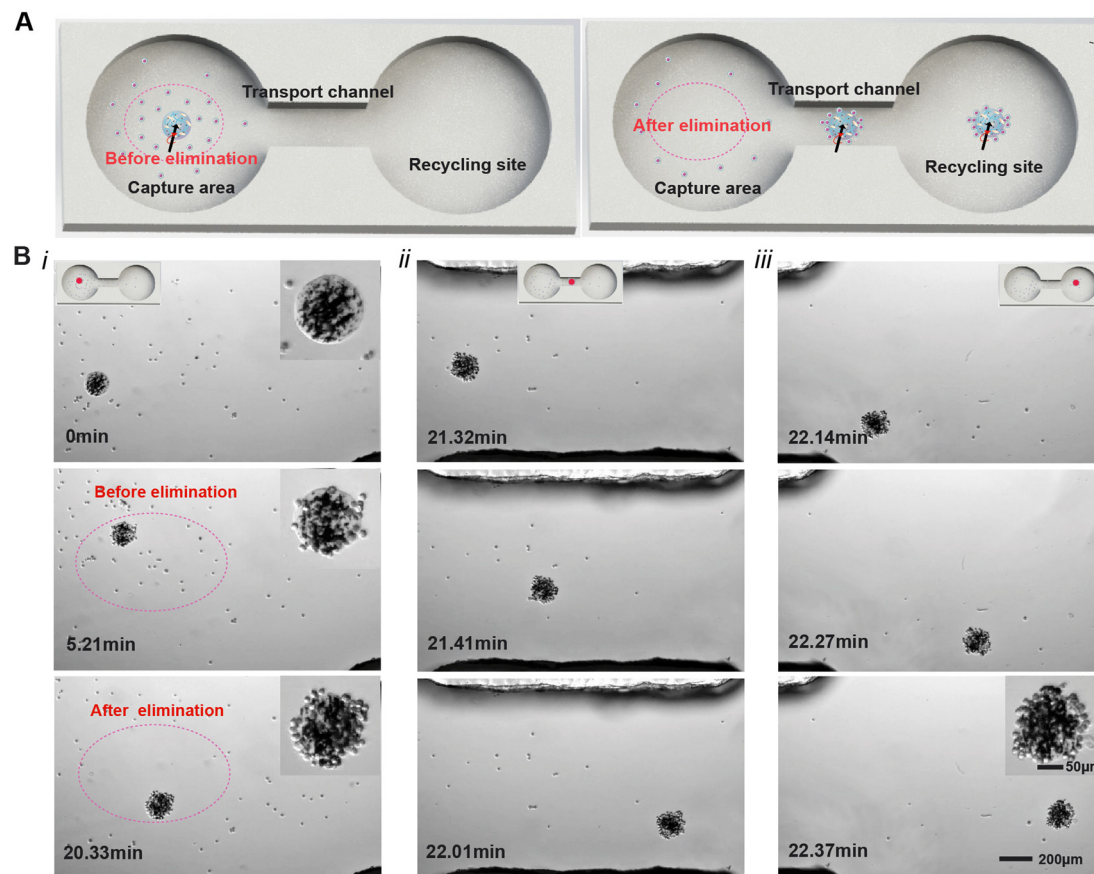
Fig. 5 Demonstration of cancer cell elimination by the magnetic ECM-mimicking microrobot in a blood vessel-mimicking microchip. (A) Schematic representation of the cancer cell elimination process, including capture and transport. (B) Time-lapse images showcasing the cancer cell elimination process. The red points indicate the locations of the magnetic ECM-mimicking microrobot as it actively captures and transports the cancer cells through the blood vessel-mimicking chip. The microrobot autonomously navigates towards the target cancer cells for effective elimination and transport. (i) Cell capturing in the predefined working region; (ii) cell transport through the connection channel; and (iii) arrival at the target recycling region.
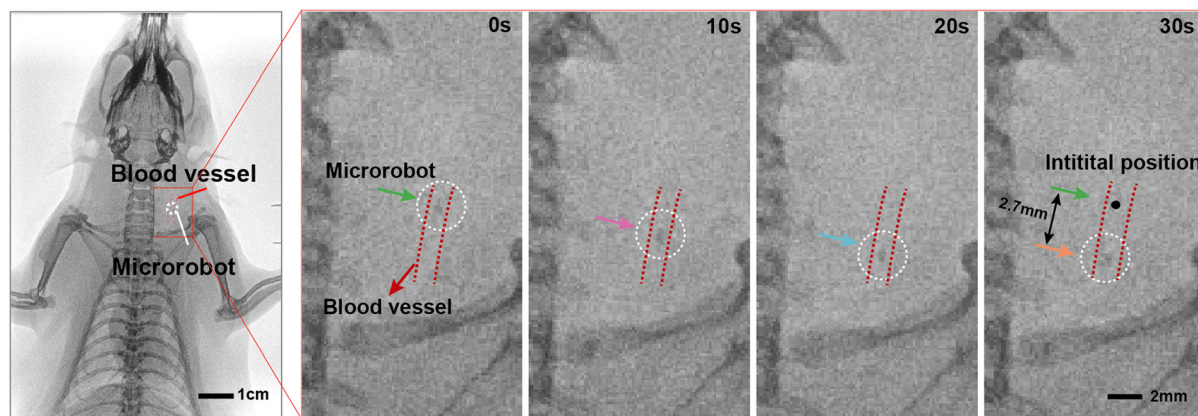

Fig. 6 *In vivo* application evaluation of the magnetic ECM-mimicking microrobot. DR images of the magnetic ECM-mimicking microrobot moving within the jugular vein of a rat under a rotating magnetic field. The red dotted line is our mark of the location of the blood vessels. The white dotted circle represents the position of the magnetic ECM-mimicking microrobot.

of *ca.* 90 μm s^{-1} driven by the external magnetic field. The microrobot moved 2.7 mm from the initial position within 30 s. These results indicate that the microrobot can overcome the complex viscoelasticity of the blood, with its size and surface properties being suitable for manoeuvring inside blood vessels. Furthermore, we evaluated the biosafety of the micro-

robot *in vivo* by continuously observing the rat over 7 days. During this period, the magnetic ECM-mimicking microrobot was retained inside the rat for later pathological analysis (Fig. S10a†). As shown Fig. S10b and Fig. S10c,† during the 7-day observation period, the appetite, sleep, and physical activity of the rat were normal. The weight of the rat remained stable over these 7 days. These results affirm the safety, controllability and active mobility of the magnetic ECM-mimicking microrobot in an *in vivo* setting, while also indicating the magnetic field's ability to safely penetrate tissue. In summary, the outcomes of our animal experiments underscore the significant potential of the magnetic ECM-mimicking microrobot for its application in blood vessels *in vivo*.

3. Conclusion

In conclusion, we have presented a magnetic ECM-mimicking microrobot based on ECM-derived HA/gelatin for effective and targeted elimination of cancer cells. The microrobot can be magnetically controlled to actively approach the target cancer cells and capture the cells through ligand–receptor interaction. Microrobots with a large size range can perform controllable movements in the cell suspension solution under the actuation of a rotating magnetic field. The ECM-mimicking microrobot exhibits high cell elimination capabilities on not only single cells but also cell clusters in both the open area filled with suspended cells and the microfluidic simulator. With its inherent biocompatibility and biodegradability, remote actuation capability, and precise cancer cell elimination, the ECM-mimicking microrobot shows tremendous potential as an effective tool for the early treatment of cancers. In future work, microrobots can be controlled in a swarm as reported previously[49] to enhance the elimination efficiency, although our current work focused on the demonstration with a single microrobot. Beyond cancer treatment, this microrobot could also be extended for targeted capture of other biological objects, such as sperm cells, to facilitate conception and open new possibilities for biomedical applications. Our work lays a solid foundation for the development of advanced microrobotic systems with broad therapeutic potential in the field of targeted cell elimination and precision medicine.

4. Methods

4.1 Materials

Gelatin and phosphate-buffered saline (PBS) were purchased from Aladdin (Shanghai, China); hyaluronic acid (HA, M_w = 1500–2500k Da) and 1-ethyl-3-(3-dimethylaminopropyl) carbodiimide (EDC) were provided by McLean (Shanghai, China); and fluorescent hyaluronic acid was purchased from Yusi Pharmaceutical Technology Co. Ltd (Chongqing, China). Magnetic particles (neodymium–iron–boron, NdFeB) were obtained from the Chengxin Alloy Material Outlet Store (Hebei, China). Bovine blood was purchased from the Wen Bai

Store (Jiangsu, China). Deionized water was prepared in our laboratory. The brands and sources of all other biochemical reagents will be mentioned in the experimental methods as described below.

4.2 Fabrication of ECM-mimicking magnetic microrobots

Magnetic ECM-mimicking microrobots were fabricated through the "interface-shearing method". First, an aqueous solution of 0.5% hyaluronic acid (HA) was continuously and fully stirred under a suitable spin speed for 1 h, and then 1-ethyl-3-(3-dimethylaminopropyl) carbodiimide (EDC) was added dropwise to the HA solution at a final concentration of 1 mg mL^{-1} to cross-link the HA. After that, we prepared a 5% gelatin solution by adding 0.7 g of gelatin with 0.1 g of NdFeB and mixing it with 0.3 g of the crosslinked HA solution at a ratio of 3 : 7 : 1. Then, the mixture was heated on a 60 °C heating plate for 0.5 h while stirring. Second, the HA/gelatin/NdFeB prepolymer was transferred to the syringe of the generator equipment, which applied a certain pressure and frequency to the syringe. Then, the syringe with a 34 G × 4 mm microneedle was plunged into 0–4 °C sunflower oil to generate HA/gelatin/NdFeB microspheres, after which the microspheres were placed at 4 °C to cool down overnight. In this experiment, gelatin is thermosensitive and the sol–gel transition temperature is about 39 °C. The liquid gelatin gradually becomes solidified when the temperature is below 39 °C. The large temperature gradient reduces the time of the sol–gel transition. A low-temperature environment of 0–4 °C based on ice bathing is used to ensure rapid solidification of the gelatin matrix. On the other hand, low temperature prevents mutual adhesion and retains the spherical shape of the microrobots. After completion, the microspheres were poured into a beaker and washed three times with detergent (the mass concentration is about 0.1 g mL^{-1}), followed by washing each three times with deionized water again to remove the oil from the surface. Third, the HA/gelatin microspheres with appropriate diameters were picked out under a microscope, and packed individually. The magnetic ECM-mimicking microrobots were obtained by placing HA/gelatin microspheres in the cylinder magnetization area of the magnetizer (RM-2070, China) for magnetization. Finally, the fabricated magnetic ECM-mimicking microrobots were stored in a fridge (4 °C) for subsequent use.

4.3 Characterization

The morphology of the prepared magnetic ECM-mimicking microrobots and the distribution of magnetic particles were observed using a microscope. The magnetic response of the prepared microrobots was verified by a permanent magnet test. The fluorescence images of the microrobots were obtained to confirm the existence of HA components. A vibrating sample magnetometer (VSM) tested the magnetic properties of the magnetic ECM-mimicking microrobots. Magnetic actuation experiments were performed by using a magnetic control system (MFG-100-i, Switzerland). The homolysis experiment tested the compatibility of the magnetic ECM-

mimicking microrobots. Zeta potential tests established the stability of the magnetic ECM-mimicking microrobots.

4.4 Cell culture

MDA-MB-231 cells (human breast cancer cell line) were cultured in a growth medium consisting of Dulbecco's modified Eagle's medium (DMEM) supplemented with 10% fetal bovine serum (FBS) and 1% antibiotic supplementation (100 U mL^{-1} penicillin and 0.1 mg mL^{-1} streptomycin). The cells were maintained in an incubator at 37 °C in 5% CO_2 mixture with ambient air to grow. We used 0.25% trypsin-EDTA in phosphate-buffered saline (PBS) to resuspend cells.

4.5 Magnetic actuation

The magnetic ECM-mimicking microrobot in this study was actuated in a magnetic control system (MFG-100-i, Switzerland) (Fig. S11†) by applying a rotating magnetic field. The magnetic control system is equipped with 8 coils located on the upper side of the region of interest (ROI) plane. In this experiment, the buffer containing the magnetic ECM-mimicking microrobot was dropped into a glass-bonded polydimethylsiloxane (PDMS) microfluidic chip, which was transferred to the ROI plane. The forward orientation is dynamically modulated by changing the axis of the rotating magnetic field according to the predetermined locomotion. The locomotion of the magnetic ECM-mimicking microrobot in the plane was observed using a microscope. The rolling motion of the magnetic ECM-mimicking microrobot was obtained by applying a rotating magnetic field of 1 or 2 mT at 0.1–0.4 Hz. We characterized the velocity of the magnetic ECM-mimicking microrobot at various actuation frequencies of the magnetic field. The microrobots with various diameters (140 μm, 200 μm, and 280 μm) were tested at 1.5 mT with frequencies ranging from 0.1 Hz to 1 Hz.

4.6 Fabrication of a microfluidic chip

A dumbbell-shaped microfluidic chip was designed to show the elimination and transportation processes of cancer cells *in vitro* (Fig. S12 and S13†). The microfluidic platform was designed as two reservoirs (diameter: 2 mm, depth: 1 mm) on both sides, which were connected *via* a bridge-like microchannel. First, the microfluidic platform was printed using a 3D printer (S3, China), and then it was put in a 12 mm × 5 mm square groove. After that, the mold was sprayed with a release agent. PDMS was mixed with a fixing agent (Dow Corning) at a ratio of 10 : 1 by weight. After that, the mixture was poured into the as-prepared mold. Furthermore, the mold with the PDMS mixture was degassed in a vacuum and cured at 60 °C for 4 h. After the O_2 plasma treatment, the PDMS channel and cleaned glass slide were bonded together through siloxane bonds to set up a microfluidic chip.

4.7 Binding with cancer cells specifically

To further certify that the magnetic ECM-mimicking microrobot has a targeting effect on tumor cells, we tested the specificity of the microrobots for combining with cancer cells in the blood. We purchased fresh bovine blood diluted with anticoagulants and removed the plasma by centrifugation. Then, 1 mL of blood was added to the PDMS chamber. After that, a small amount of cancer cells was added to the blood. Finally, the magnetic ECM-mimicking microrobot was injected into the PDMS chamber. The microfluidic chip was transferred to the magnetic control system. The magnetic ECM-mimicking microrobot captures cancer cells in the blood at 0.3–0.5 Hz and 3 mT.

4.8 Targeted elimination of cancer cells

Experiments involving the capture and transport of MDA-MB-231 cells under magnetic actuation were performed. First, MDA-MB-231 cells were maintained in DMEM at 37 °C under a humidified atmosphere with 5% CO_2. Second, the microfluidic chip as prepared before was sterilized with ultraviolet light. Then, a cancer cell culture medium of DMEM was added to fill the whole microfluidic chip. After that, a small amount of cancer cells was injected into the left chamber of the microfluidic chip. The channel and the right chamber were free of cancer cells. Second, we used a pipette to place the magnetic ECM-mimicking microrobot into the left chamber of the microfluidic chip and covered it with a glass slide (Fig. S13†). Finally, the microfluidic chip was transferred to the magnetic control system. The forward orientation was controlled by modulating dynamically the axis of rotation, which guided the magnetic ECM-mimicking microrobot to approach and capture the cancer cells. Then, the magnetic ECM-mimicking microrobot with captured cancer cells is moved along the channel to the right chamber.

4.9 Cell viability

Cytotoxicity was investigated by incubating the magnetic ECM-mimicking microrobot with MDA-MB-231 cells and assessed using a live/dead staining assay. MDA-MB-231 human breast cancer cells were seeded into a well of a 48-well plate and cultured in DMEM. The medium was supplemented with 10% fetal bovine serum (FBS) and 100 U mL^{-1} penicillin/streptomycin. After 12 h, the magnetic ECM-mimicking microrobots were loaded into the wells. The medium in the well was refreshed every 24 hours. To characterize the viability, cells were stained using the Live/Dead Cell Assay kit (Sigma-Aldrich, China) for 15 min at 37 °C. After washing twice with a PBS buffer, the cells were then observed and mounted under a fluorescence microscope.

4.10 Animal experiments

Animal experiments were conducted through procedures approved by the Animal Experiment Ethics Committee of TOP (approval no. TOP-IACUC-2023-0118). An SD rat (20–21 weeks of age, male, 394 g) was purchased from To Pu Biotechnology Co., Ltd in China. The magnetic ECM-mimicking microrobot as prepared before was soaked in PBS and sterilized with ultraviolet light for 1 h. The rat was anesthetized after injecting a mixture of ketamine (70 mg kg^{-1}) and xylazine (7 mg kg^{-1}). The rat was fixed on a sterile surgical board after anesthetiz-

ing. Then, its neck skin was cut with surgical scissors, and its subcutaneous tissue was bluntly separated with surgical forceps to expose the left side. After freeing the blood vessels using microscopic forceps, the proximal and distal ends of the peripheral venous vessels of the rat were ligated, leaving about 1 cm of blood vessels. As shown in Fig. S9,† the microrobot with a diameter of 500 μm was injected into the jugular vein of the rat. The magnetic ECM-mimicking microrobot was actuated under a rotating magnetic field at a frequency of 6 Hz. The DR imaging equipment was used to monitor the locomotion of the microrobot in the vessels. The position changes of the magnetically driven microrobot were recorded every 10 seconds using DR imaging. After that, the magnetic ECM-mimicking microrobot was kept in the rat to evaluate its biosafety *in vivo*. As shown in Fig. S10a,† we sutured the skin of the rat's neck wound, and the rat was disinfected with iodine and put back into its cage. After the rat regained consciousness, it was transferred to the breeding room. We conducted a pathological analysis of the rat during 7 days of treatment, and we recorded the rat's status and weighed it every day.

Author contributions

H. X. conceived the project. H. X. and F. D. designed the research with the help of J. H. and Y. L. J. H and Y. L. performed the experimental work with help from C. L., J. W., J. L., N. W., X. L. and L. W. All authors wrote the paper and participated in the discussions.

Conflicts of interest

There are no conflicts to declare.

Acknowledgements

References

1 A. Weth, I. Krol, K. Priesner, C. Donato, S. Pirker, C. Wolf, N. Aceto and W. Baumgartner, *Sci. Rep.*, 2020, **10**, 10181.

2 A. F. Chambers, A. C. Groom and I. C. MacDonald, *Nat. Rev. Cancer*, 2002, **2**, 563–572.

3 J. P. Thiery, H. Acloque, R. Y. Huang and M. A. Nieto, *Cell*, 2009, **139**, 871–890.

4 G. P. Gupta and J. Massague, *Cell*, 2006, **127**, 679–695.

5 S. Gkountela and N. Aceto, *Biol. Direct*, 2016, **11**, 33.

6 S. Gkountela, B. Szczerba, C. Donato and N. Aceto, *ESMO Open*, 2016, **1**, e000078.

7 D. Lin, L. Shen, M. Luo, K. Zhang, J. Li, Q. Yang, F. Zhu, D. Zhou, S. Zheng, Y. Chen and J. Zhou, *Signal Transduction Targeted Ther.*, 2021, **6**, 404.

8 N. Behranvand, F. Nasri, R. Zolfaghari Emameh, P. Khani, A. Hosseini, J. Garssen and R. Falak, *Cancer Immunol. Immunother.*, 2022, **71**, 507–526.

9 Z. Y. Tan, *Med. Sci. Monit.*, 2019, **25**, 3537–3541.

10 Z. Zhang, X. Liu, D. Chen and J. Yu, *Signal Transduction Targeted Ther.*, 2022, **7**, 258.

11 H. Xu, M. Medina-Sanchez, W. Zhang, M. P. H. Seaton, D. R. Brison, R. J. Edmondson, S. S. Taylor, L. Nelson, K. Zeng, S. Bagley, C. Ribeiro, L. P. Restrepo, E. Lucena, C. K. Schmidt and O. G. Schmidt, *Nanoscale*, 2020, **12**, 20467–20481.

12 J. Hou, X. Liu and S. Zhou, *View*, 2021, **2**, 20200023.

13 Y. Ma, X. Tian, L. Liu, J. Pan and G. Pan, *Acc. Chem. Res.*, 2019, **52**, 1611–1622.

14 L. Yu, P. Tang, C. Nie, Y. Hou and R. Haag, *Adv. Healthc. Mater.*, 2021, **10**, e2002202.

15 S. Amorim, C. A. Reis, R. L. Reis and R. A. Pires, *Trends Biotechnol.*, 2021, **39**, 90–104.

16 J. Nicolas, S. Magli, L. Rabbachin, S. Sampaolesi, F. Nicotra and L. Russo, *Biomacromolecules*, 2020, **21**, 1968–1994.

17 J. M. Viola, C. M. Porter, A. Gupta, M. Alibekova, L. S. Prahl and A. J. Hughes, *Adv. Mater.*, 2020, **32**, e2002195.

18 J. Pan, W. Chen, Y. Ma and G. Pan, *Chem. Soc. Rev.*, 2018, **47**, 5574–5587.

19 W. P. Daley, S. B. Peters and M. Larsen, *J. Cell Sci.*, 2008, **121**, 255–264.

20 A. G. Tavianatou, I. Caon, M. Franchi, Z. Piperigkou, D. Galesso and N. K. Karamanos, *FEBS J.*, 2019, **286**, 2883–2908.

21 J. Lesley, V. C. Hascall, M. Tammi and R. Hyman, *J. Biol. Chem.*, 2000, **275**, 26967–26975.

22 M. D. Mager, V. LaPointe and M. M. Stevens, *Nat. Chem.*, 2011, **3**, 582–589.

23 O. Chaudhuri, J. Cooper-White, P. A. Janmey, D. J. Mooney and V. B. Shenoy, *Nature*, 2020, **584**, 535–546.

24 X. Jia, K. Minami, K. Uto, A. C. Chang, J. P. Hill, J. Nakanishi and K. Ariga, *Adv. Mater.*, 2020, **32**, e1905942.

25 X. Tian, X. Sha, Y. Feng, Y. Duan, M. Dong, L. Liu and G. Pan, *ACS Appl. Mater. Interfaces*, 2019, **11**, 41019–41029.

26 W. He, Z. Yao, Y. Diao, M. Wang and G. Pan, *Mater. Chem. Front.*, 2023, **7**, 4050–4062.

27 K. Xiong, W. Wei, Y. Jin, S. Wang, D. Zhao, S. Wang, X. Gao, C. Qiao, H. Yue, G. Ma and H. Y. Xie, *Adv. Mater.*, 2016, **28**, 7929–7935.

28 H. Shen, S. Cai, Z. Wang, Z. Ge and W. Yang, *Mater. Des.*, 2023, **227**, 111735.

29 X.-Z. Chen, M. Hoop, F. Mushtaq, E. Siringil, C. Hu, B. J. Nelson and S. Pané, *Appl. Mater. Today*, 2017, **9**, 37–48.

30 H. Zhou, C. C. Mayorga-Martinez, S. Pane, L. Zhang and M. Pumera, *Chem. Rev.*, 2021, **121**, 4999–5041.

31 M. Koleoso, X. Feng, Y. Xue, Q. Li, T. Munshi and X. Chen, *Mater. Today Bio*, 2020, **8**, 100085.

32 C. Xu, Z. Yang and G. Z. Lum, *Adv. Mater.*, 2021, **33**, e2100170.

33 C. Xin, D. Jin, Y. Hu, L. Yang, R. Li, L. Wang, Z. Ren, D. Wang, S. Ji, K. Hu, D. Pan, H. Wu, W. Zhu, Z. Shen, Y. Wang, J. Li, L. Zhang, D. Wu and J. Chu, *ACS Nano*, 2021, **15**, 18048–18059.

34 H. Xu, M. Medina-Sánchez and O. G. Schmidt, *Angew. Chem., Int. Ed.*, 2020, **59**, 15029–15037.

35 J. Vyskocil, C. C. Mayorga-Martinez, E. Jablonska, F. Novotny, T. Ruml and M. Pumera, *ACS Nano*, 2020, **14**, 8247–8256.

36 T. Bhuyan, A. T. Simon, S. Maity, A. K. Singh, S. S. Ghosh and D. Bandyopadhyay, *ACS Appl. Mater. Interfaces*, 2020, **12**, 43352–43364.

37 Y. Liu, G. Lin, G. Bao, M. Guan, L. Yang, Y. Liu, D. Wang, X. Zhang, J. Liao, G. Fang, X. Di, G. Huang, J. Zhou, Y. Y. Cheng and D. Jin, *ACS Nano*, 2021, **15**, 19924–19937.

38 C. C. Mayorga-Martinez, M. Fojtů, J. Vyskočil, N. J. Cho and M. Pumera, *Adv. Funct. Mater.*, 2022, **32**, 2207272.

39 K. Villa, L. Krejčová, F. Novotný, Z. Heger, Z. Sofer and M. Pumera, *Adv. Funct. Mater.*, 2018, **28**, 1804343.

40 P. Wrede, O. Degtyaruk, S. K. Kalva, X. L. Dean-Ben, U. Bozuyuk, A. Aghakhani, B. Akolpoglu, M. Sitti and D. Razansky, *Sci. Adv.*, 2022, **8**, eabm9132.

41 D. L. Wise, *Handbook of Pharmaceutical Controlled Release Technology*, 2000.

42 J. A. Burdick and G. D. Prestwich, *Adv. Mater.*, 2011, **23**, H41–H56.

43 J. Y. Lai, D. H. Ma, H. Y. Cheng, C. C. Sun, S. J. Huang, Y. T. Li and G. H. Hsiue, *J. Biomater. Sci., Polym. Ed.*, 2010, **21**, 359–376.

44 Y. Liu, G. Lin, Y. Chen, I. Monch, D. Makarov, B. J. Walsh and D. Jin, *Lab Chip*, 2020, **20**, 4561–4571.

45 R. Bernasconi, E. Mauri, A. Rossetti, S. Rimondo, R. Suriano, M. Levi, A. Sacchetti, S. Pané, L. Magagnin and F. Rossi, *Mater. Des.*, 2021, **197**, 109212.

46 T. L. Wang, H. Ugurlu, Y. B. Yan, M. T. Li, M. Li, A. M. Wild, E. Yildiz, M. Schneider, D. Sheehan, W. Q. Hu and M. Sitti, *Nat. Commun.*, 2022, **13**, 4465.

47 B. Wang, K. F. Chan, K. Yuan, Q. Q. Wang, X. F. Xia, L. D. Yang, H. Ko, Y. X. J. Wang, J. J. Y. Sung, P. W. Y. Chiu and L. Zhang, *Sci. Robot*, 2021, **6**, eabd2813.

48 M. Zhang, R. Guo, K. Chen, Y. Wang, J. Niu, Y. Guo, Y. Zhang, Z. Yin, K. Xia, B. Zhou, H. Wang, W. He, J. Liu, M. Sitti and Y. Zhang, *Proc. Natl. Acad. Sci. U. S. A.*, 2020, **117**, 14667–14675.

49 H. Xie, M. M. Sun, X. J. Fan, Z. H. Lin, W. N. Chen, L. Wang, L. X. Dong and Q. He, *Sci. Robot*, 2019, **4**, eaav8006.